

Strain energy density in the x-ray powder diffraction from mixed crystals and alloys

Yu Rosenberg^{†§}, V Sh Machavariani[†], A Voronel[†], S Garber[†], A Rubshtein[†],
A I Frenkel^{‡||} and E A Stern[‡]

[†] School of Physics and Astronomy, Raymond and Beverly Sackler Faculty of Exact Sciences,
Tel-Aviv University, 69978, Tel-Aviv, Israel

[‡] Physics Department, Box 351560, University of Washington, Seattle, WA 98195-1560, USA

Received 12 May 2000, in final form 12 July 2000

Abstract. A correlation between precise x-ray powder diffraction patterns and atomic size mismatch in disordered mixed crystals (alloys and ionic crystals) is observed. The anisotropy of the elastic moduli has been taken into account for evaluation of the strain energy density of the mixed crystals revealed in x-ray powder diffraction measurements. The precursor of the phase transformation for a quenched disordered Au–Cu alloy is identified.

1. Introduction

It is widely accepted that in the first approximation the lattice parameter of a mixed crystal or alloy varies linearly with the composition (Vegard's law). The real structures deviate from this oversimplified view considerably. In our extended study of mixed ionic salts with atomic size mismatch, RbBr–KBr [1, 2], RbCl–RbBr [1–3], and AgCl–AgBr [4], strong deviations of the local structure obtained by the x-ray absorption fine-structure (XAFS) technique from the average structure obtained by x-ray powder diffraction (XRPD) measurements have been revealed. The equilibrium atomic positions have been found by the XAFS analysis to be shifted from the periodic lattice sites, ascertained by means of diffraction. Our further XAFS investigation of the disordered metallic alloy Au_xCu_{1-x} (reference [5]) also reveals considerable deviations of the interatomic distances from averaged ones measured using XRPD. In our present careful XRPD investigation we are trying to find the characteristic features of diffraction patterns of crystals with disorder ascertained from the XAFS.

Earlier [6], the diffuse scattering of the ordered Cu_3Au alloys was extensively studied. In this paper, the alloys with random distribution of the atoms within the crystal lattice are investigated. Typical diffuse intensities [7] are several orders of magnitude below the Bragg peak intensities. Therefore, an investigation of the diffuse scattering demands very high signal-to-noise ratio. In the present work we use the width and position of the Bragg peak itself. This experiment is simpler because of the large Bragg peak intensities. Another feature of our research is that we have used the XRPD measurement technique which is easier to do than using single-crystal x-ray diffraction. Another advantage of the powder diffraction technique is that it can be applied to a wider range of materials (because it does not need

§ Present address: Wolfson Centre for Materials Research, Tel-Aviv University, 69978, Israel.

|| Present address: Materials Research Laboratory, University of Illinois at Urbana-Champaign, USA.

a single crystal) than the usual (single-crystal) x-ray diffraction technique. This might be especially important for thin-film growth monitoring and for the investigation of the properties of cold-rolled steels. The linewidths as a function of diffraction angle have been carefully measured for different concentrations for Au–Cu, Au–Ag, RbBr–RbCl, and AgBr–AgCl. It has been found that a definite correlation exists between the built-in atomic size disorder and the XRPD line broadening in all the mixed crystals investigated. Thus, this paper outlines a simple phenomenological method for investigation of the macroscopic consequence (strain energy density) of the local disorder.

2. Experimental procedure

The Au–Cu alloys were quenched to avoid phase separation. The details of the sample preparation were presented in references [1–5]. Homogeneity of the alloys and mixtures was verified by means of XRPD and no traces of phase separation or superstructure were observed for any of the concentrations. The compositions of the mixed samples were established by energy-dispersive spectroscopy with a scanning electron microscope. All specimens were found to be homogeneous within the accuracy of 1%.

XRPD data were collected in the range 30–120° (2 Θ range) with Cu K α radiation on the Θ : Θ powder diffractometer ‘Scintag’ equipped with a liquid-nitrogen-cooled Ge solid-state detector. Peak positions and widths of Bragg reflections were determined by a self-consistent profile-fitting technique using the Pearson VII function [8]. The contributions of K α_2 radiation were subtracted from the total profiles; the results obtained correspond to just the K α_1 component of the K α doublet. Lattice constant computation was carried out by a reciprocal-lattice-parameter refinement. The lattice constants determined are presented in figures 1(a) and 2(a) as deviations from Vegard’s law.

The Williamson–Hall [9] approach allows us to separate two different causes for a line broadening. It is usually assumed [10] that the broadening β_τ of a Bragg reflection (hkl) originating from the finite grain size of the polycrystal follows the Sherrer equation:

$$\beta_\tau = \frac{\lambda}{\tau \cos \Theta_{hkl}} \quad (1)$$

where λ is the x-ray wavelength, Θ_{hkl} is a Bragg angle, and τ is a mean ‘effective’ size of the coherent scattering region normal to the reflecting planes.

If this is the only reason for the broadening, then the value $\beta_\tau \cos \Theta_{hkl}$ should be independent of the diffraction angle. However, the real situation is different, because of the persistence of the additional stress-induced broadening β_ε which is given by the Wilson formula:

$$\beta_\varepsilon = 4\varepsilon \tan \Theta_{hkl}. \quad (2)$$

Here ε is a dimensionless value (‘microstrain’) which is usually assumed to be proportional to the square root of the density of dislocations. Assuming that the contributions to the Bragg peak are mutually independent and both have a Cauchy-like profile, one gets, for the total reflection width β_{hkl} ,

$$\beta_{hkl} = \beta_\tau + \beta_\varepsilon = \frac{\lambda}{\tau \cos \Theta_{hkl}} + 4\varepsilon \tan \Theta_{hkl}. \quad (3)$$

Plotting now the measured value $\beta_{hkl} \cos \Theta_{hkl}$ as a function of the argument $4 \sin \Theta_{hkl}$, one can estimate the microstrain ε from the slope of the line and τ from its intersection with the vertical axis.

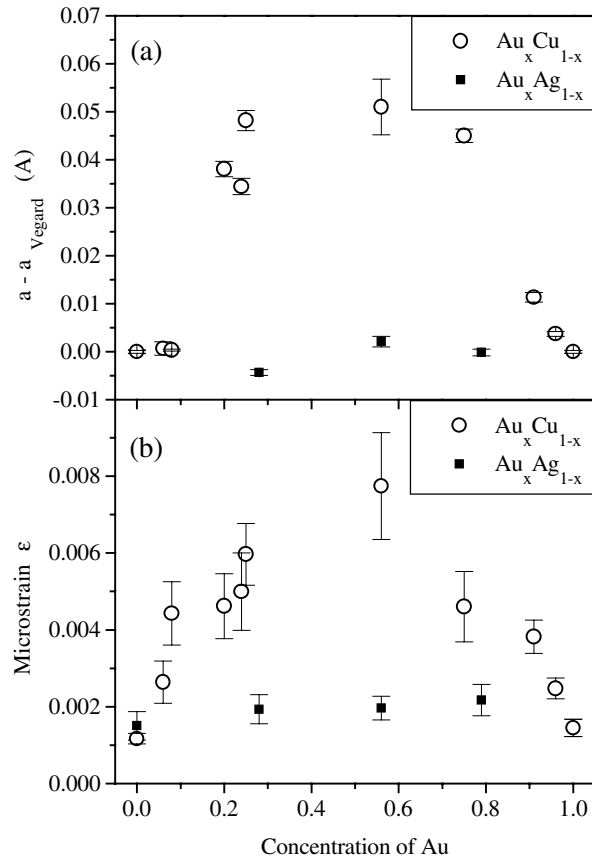


Figure 1. (a) The lattice parameter for Au_xCu_{1-x} and Au_xAg_{1-x} metallic alloys presented as a deviation from Vegard's law, $a - a_{Vegard}$. (b) The microstrain ϵ as determined by means of XRPD for Au_xCu_{1-x} and Au_xAg_{1-x} metallic alloys.

3. Results and discussion

The microstrains ϵ obtained are presented in figures 1(b) and 2(b). It should be pointed out that our experimental widths are not corrected for instrumental broadening. Therefore, the values of microstrains measured for the pure components give us the instrumental zero points.

Let us try to probe deeper. Equations (2) and (3) assume that the microstrain ϵ is uniform in all crystallographic directions. This assumption is doubtful for a crystalline material. It is more physical to consider an anisotropic magnitude ϵ_{hkl} . In reference [11] a uniform stress (deformation pressure) σ was assumed. In this case, ϵ in equations (2) and (3) has to be replaced by an anisotropic microstrain $\epsilon_{hkl} = \sigma/E_{hkl}$, where E_{hkl} is the Young's modulus in direction hkl . Equation (3) transforms into equation (4):

$$\beta_{hkl} = \beta_{\tau} + \beta_{\epsilon} = \frac{\lambda}{\tau \cos \Theta_{hkl}} + 4\sigma \tan \Theta_{hkl} / E_{hkl}. \quad (4)$$

However, it may be more reasonable to expect the real parameter for the deformation to be a density of a deformation energy u . Thus, assuming this density to be uniform, $u = \epsilon_{hkl}^2 E_{hkl} / 2$ (Hooke's law), one has to substitute for ϵ in equations (2) and (3) the anisotropic microstrain

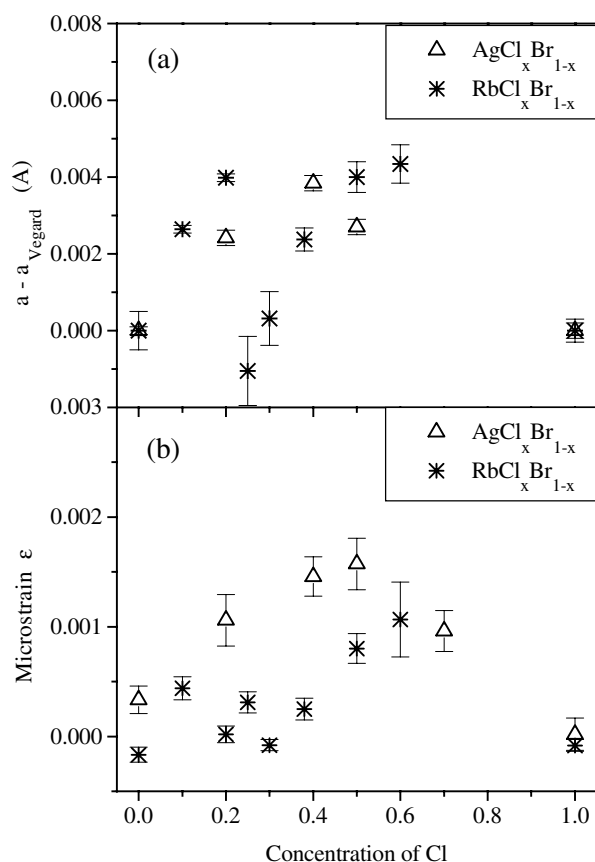


Figure 2. (a) The lattice parameter for $\text{AgCl}_x\text{Br}_{1-x}$ and $\text{RbCl}_x\text{Br}_{1-x}$ ionic crystals presented as a deviation from Vegard's law, $a - a_{\text{Vegard}}$. (b) The microstrain ϵ as determined by means of XRPD for $\text{AgCl}_x\text{Br}_{1-x}$ and $\text{RbCl}_x\text{Br}_{1-x}$ ionic crystals.

$\epsilon_{hkl} = \sqrt{2u/E_{hkl}}$. As a result one obtains the following equation:

$$\beta_{hkl} = \frac{\lambda}{\tau \cos \Theta_{hkl}} + \left(4 \sqrt{\frac{2}{E_{hkl}}} \tan \Theta_{hkl} \right) \sqrt{u}. \quad (5)$$

Figures 3 and 4 present the comparisons of these three evaluation procedures for the $\text{Au}_{0.20}\text{Cu}_{0.80}$ and $\text{Au}_{0.56}\text{Ag}_{0.44}$ alloys, respectively. Figures 3(a) and 4(a) correspond to equation (3), figures 3(b) and 4(b) correspond to equation (4), figures 3(c) and 4(c) correspond to equation (5). The Young's moduli E_{hkl} for the cubic crystals [12] were calculated using a linear interpolation of data from reference [13]. The scattering of the points away from the linear expression is much less for the parts (c). All of the other concentrations exhibit analogous behaviour. Therefore, the assumption of uniform deformation energy is found to be better for the metallic samples. As for the mixed salts, the broadening effect is an order of magnitude smaller and is too small for a significant difference between the approaches to be seen.

Figure 5 presents the calculated density of the deformation energy for the metallic (part (a)) and non-metallic (part (b)) samples. One can see from both parts that the maximal deformation energy density roughly corresponds to the 50–50 concentration range. In substitutionally

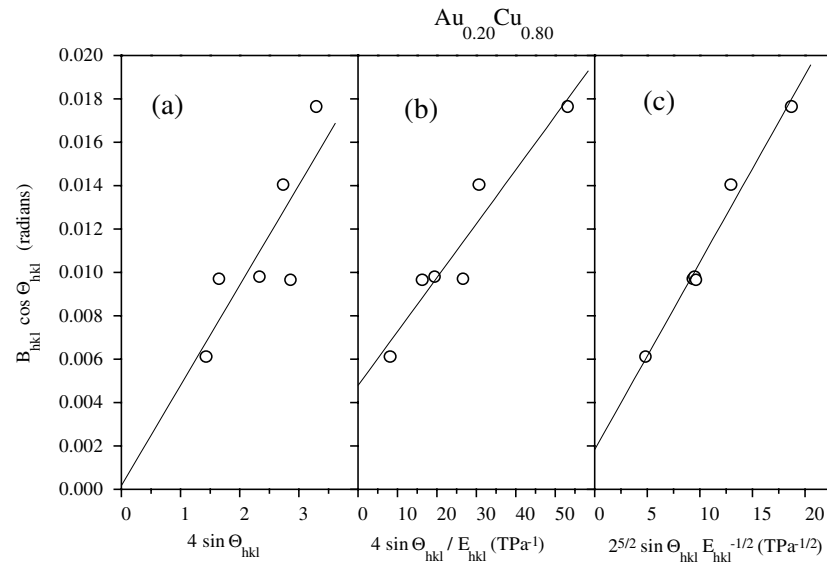


Figure 3. The analysis of the angular dependence of the Bragg peak widths on the assumption of a uniform deformation ε (a), uniform stress σ (b), and uniform deformation energy u (c) for $\text{Au}_{0.20}\text{Cu}_{0.80}$ alloy.

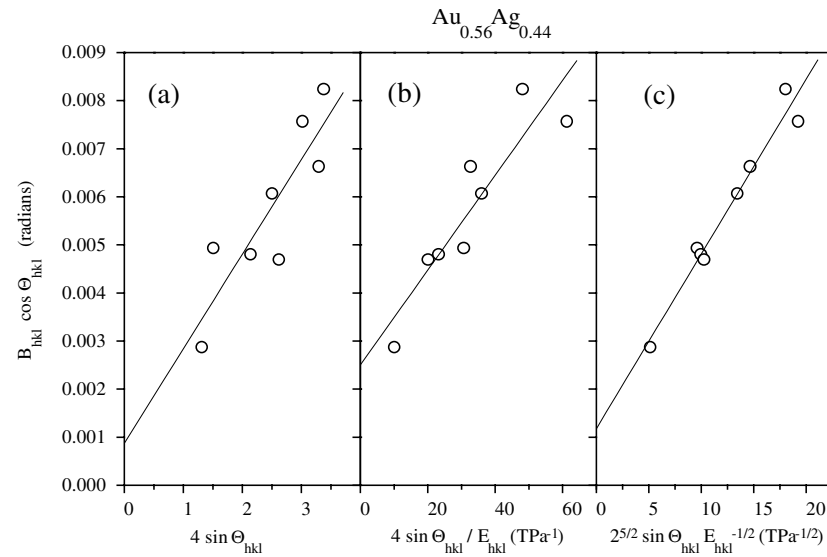


Figure 4. The analysis of the angular dependence of the Bragg peak widths on the assumption of a uniform deformation ε (a), uniform stress σ (b), and uniform deformation energy u (c) for $\text{Au}_{0.56}\text{Ag}_{0.44}$ alloy.

disordered crystal, each site may be occupied either by an atom of size d_1 or by one of size d_2 with probabilities $1 - x$ and x respectively. The relative size dispersion γ can be written as [14]

$$\gamma = \frac{\langle(\Delta d)^2\rangle}{\langle d \rangle^2} = \frac{(1-x)d_1^2 + xd_2^2 - ((1-x)d_1 + xd_2)^2}{((1-x)d_1 + xd_2)^2} = x(1-x) \frac{(d_1 - d_2)^2}{\langle d \rangle^2}. \quad (6)$$

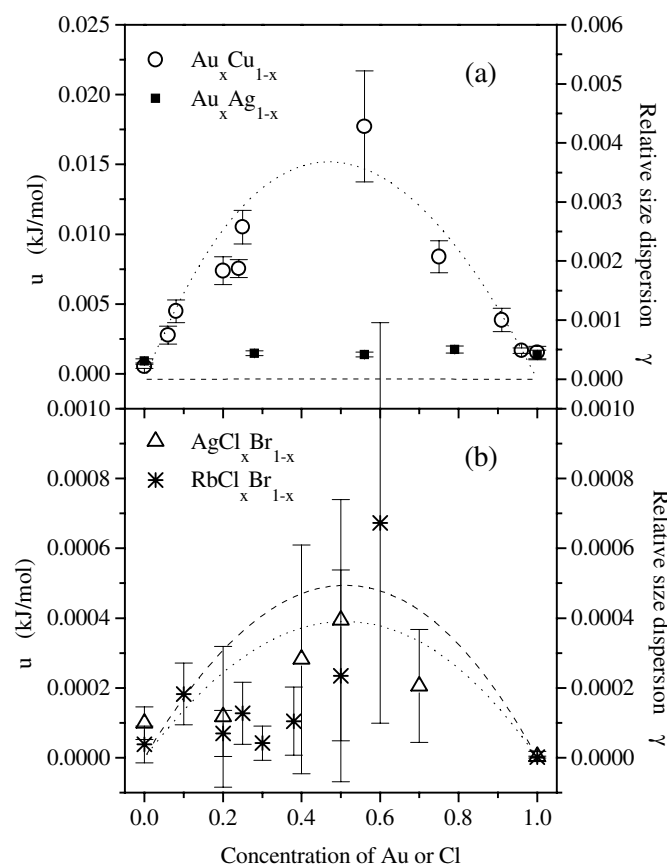


Figure 5. (a) The density of the deformation energy u for $\text{Au}_x\text{Cu}_{1-x}$ and $\text{Au}_x\text{Ag}_{1-x}$ metallic alloys. Dotted (Au–Cu) and dashed (Au–Ag) curves show the relative size dispersion γ (right-hand scale). (b) The density of the deformation energy u for $\text{AgCl}_x\text{Br}_{1-x}$ and $\text{RbCl}_x\text{Br}_{1-x}$ ionic crystals. Dotted (AgCl–AgBr) and dashed (RbCl–RbBr) curves show the relative size dispersion γ (right-hand scale).

Indeed, this dispersion has a maximum at 50–50 concentration, independently of the disparity in size, but its maximal value is greater for greater disparity. In the case of ionic crystal, the distance between anions is the corresponding relevant parameter. Figure 5 demonstrates the correlation between the density of the deformation energy and the size dispersion. In spite of the fact that the relative size dispersion (and, simultaneously, the deformation energy) within the ionic crystals is about an order of magnitude less than in the metallic alloys and is within the uncertainty of our measurements, the results do not contradict a definite correlation between u and the size dispersion.

The anisotropy of the microstrains is compatible with our results presented in figure 6 for the lattice parameters a_{hkl} of the Au–Cu alloys evaluated from the positions of the different individual Bragg reflections. The set of a_{hkl} has been calculated for every sample from the lattice spacings of the corresponding Bragg reflections. The deviations of the lattice parameters for different planes from the average depend systematically on the concentration. The difference grows rapidly in the middle of the concentration range, while this effect disappears for pure Au and Cu. This means that the effect considerably exceeds the uncertainty of the measurement. Let us stress here the difference in experimental origin of figures 5 and 6.

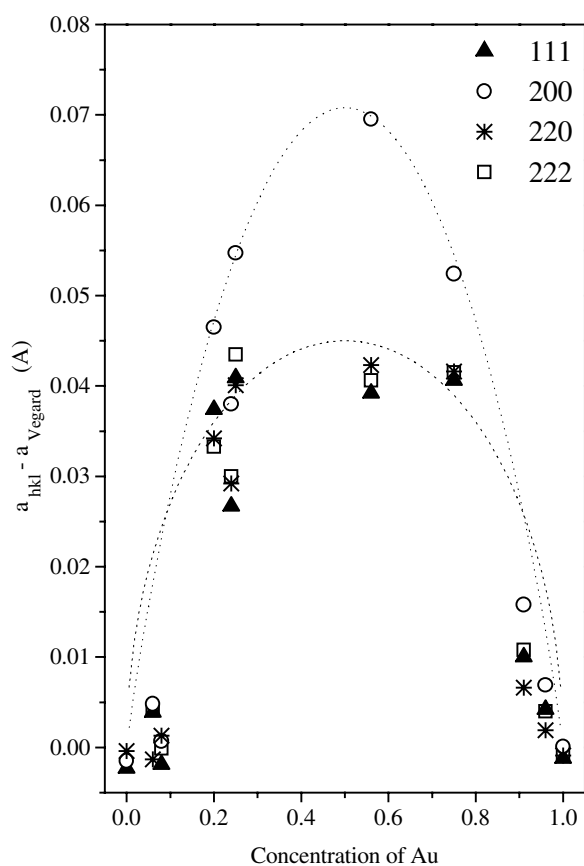


Figure 6. The lattice parameter a_{hkl} evaluated from the positions of the different individual Bragg reflections (presented as a deviation from Vegard's law, $a_{hkl} - a_{Vegard}$) for Au_xCu_{1-x} metallic alloy.

While the microstrains are determined by the analysis of the XRPD peak widths, the lattice parameters a_{hkl} for different crystallographic planes are determined from the positions of the peaks. Therefore, figures 5 and 6 present the results from two independent experimental techniques.

The result presented in figure 6 originates, probably, from the different macroscopic deformations within the grains in different crystallographic directions. This discrepancy is maximal between (111) and (200) planes. It is compatible with the greater stiffness of the direction [111] (space diagonal) in the Au–Cu alloys [12, 13]. Thus, deformation (expansion) in the direction [200] is easier. Such a difference between the lattice parameters for the different crystallographic planes may be considered as a precursor of a phase transformation of the Au–Cu alloy from the metastable disordered fcc phase to the two separate phases of pure (or, probably, Cu_3Au and Au) components.

The difference in $a_{hkl} - a_{Vegard}$ between the (200) and the other (hkl) diffraction peaks is in apparent disagreement with *macroscopic* cubic symmetry. However, the broadening of the diffraction lines indicates that there is no perfect long-range order, due to the limited mean 'effective' size of the coherent scattering region normal to the reflecting planes and an anisotropic microstrain ϵ_{hkl} . Both of these effects broaden the diffraction peaks, destroying the long-range cubic symmetry, allowing the microstrains to violate cubic symmetry *locally*.

Another aspect of the results presented here to be noted is that the Au–Cu alloys were rapidly quenched to avoid thermal equilibrium ordering and phase separation, while the Au–Ag

alloy and the mixed salts were cooled more slowly, since their disordered phases are thermally stable. Thus, one expects the quenched alloy to have higher strains than the others, as observed. The microstrains are an inherent feature of the non-thermal equilibrium quenched state, and any attempt to remove them by annealing would cause the alloy to change phase. These microstrains are an inherent feature of the disordered alloy at lower temperatures and their large magnitude is related to the large relative atomic size disparity in the disordered Au–Cu alloys. The energy associated with the microstrains is the important factor in making the disordered phase of Au–Cu alloys thermally unstable at lower temperatures.

4. Conclusions

A definite correlation exists between both the line positions and the linewidths of the XRPD pattern and the relative atomic size disparity of the disordered mixed crystals Au–Cu, Au–Ag, AgCl–AgBr, and RbCl–RbBr.

Different ways to take account of the elastic anisotropy of the crystals are compared. It is found that the suggested concept of a uniform density of the strain energy u gives the most adequate presentation of our experimental XRPD data on the alloys. This strain energy density depends on concentration in the same way as the relative atomic size dispersion.

The difference between the lattice parameters of Au–Cu alloy evaluated from the different Bragg reflections (200) and (111) depends on concentration in a systematic way. This difference is interpreted as a precursor of the phase transformation.

Acknowledgments

This work was partially supported by The Aaron Gutwirth Foundation, Allied Investments Limited (Israel), by DOE Grant No DE-FG02-96ER45439 through the Materials Research Laboratory at the University of Illinois at Urbana-Champaign (AIF), and by DOE Grant No DE-FG03-98ER45681 through the University of Washington, Seattle (AIF and EAS).

References

- [1] Frenkel A I, Stern E A, Voronel A, Qian M and Newville M 1993 *Phys. Rev. Lett.* **71** 3485
- [2] Frenkel A I, Stern E A, Voronel A, Qian M and Newville M 1994 *Phys. Rev. B* **49** 11 662
- [3] Frenkel A I, Stern E A, Voronel A and Heald S 1996 *Solid State Commun.* **99** 67
- [4] Frenkel A I, Voronel A, Katzir A, Newville M and Stern E A 1995 *Physica B* **208+209** 334
- [5] Frenkel A I, Stern E A, Rubshtein A, Voronel A and Rosenberg Yu 1997 *J. Physique Coll.* IV **7** C2 1005
Frenkel A I, Machavariani V Sh, Rubshtein A, Rosenberg Yu, Voronel A and Stern E A 2000 Local structure of disordered Au–Cu alloys, in preparation
- [6] Cowley J M 1950 *J. Appl. Phys.* **21** 24
Warren B E, Averbach B L and Roberts B W 1951 *J. Appl. Phys.* **22** 1493
- [7] Welberry T R and Butler B D 1995 *Chem. Rev.* **95** 2369
- [8] Langford J and Louër D 1996 *Rep. Prog. Phys.* **59** 131
- [9] Williamson G K and Hall W H 1953 *Acta Metall.* **1** 22
- [10] Klug H P and Alexander L E 1974 *X-Ray Diffraction Procedures for Polycrystalline and Amorphous Materials* (New York: Wiley)
- [11] Reimann K and Würschum R 1997 *J. Appl. Phys.* **81** 7186
- [12] Love A E H 1944 *A Treatise on the Mathematical Theory of Elasticity* (New York: Dover)
For cubic crystals, Young's modulus E_{hkl} for the $[hkl]$ direction has the form $E_{hkl}^{-1} = s_{11} - (2s_{11} - 2s_{12} - s_{44})(k^2l^2 + l^2h^2 + h^2k^2)/(h^2 + k^2 + l^2)^2$, where s_{11} , s_{12} , and s_{44} are elastic compliances.
- [13] *Landolt-Börnstein New Series* 1979 vol 11 (Berlin: Springer)
- [14] Voronel A, Rabinovich S, Kisliuk A, Steinberg V and Sverbilova T 1988 *Phys. Rev. Lett.* **60** 2402